# An Experimental Investigation on the Kinetics of Solute Driven Remelting

B. DUTTA and M. RETTENMAYR

The present study is aimed at understanding the interface kinetics during solute driven remelting in metallic alloys. Solid Al is placed in contact with a liquid Al-Mg alloy. As solid and liquid compositions at the interface are out of equilibrium, remelting takes place. The remelting rate is estimated as a function of time using a simple heat balance. The estimated velocity from the heat-balance calculations shows excellent agreement with the geometric velocity, directly measured from the remelted samples in each experiment. This confirms the accuracy and reliability of the heat-balance calculations and establishes this technique as a potential method for tracing the interface velocity during remelting. The results indicate that, at a constant temperature, an increase in liquid supersaturation leads to a linear increase in remelting velocity, as a result of an increasing driving force for remelting. At a constant liquid supersaturation, an increase in temperature results in an exponential increase in the remelting velocity, due to the enhanced mass transport at the higher temperatures. Semi-empirical relations are derived from these experimental observations and a combined analysis of the effects of driving force and kinetics yields a relation for remelting velocity as a function of temperature for a variety of boundary conditions. Remelting velocities predicted by this relation are in good agreement with the experimental observations.

## I. INTRODUCTION

THE melting of a metal or a metal alloy is an important phenomenon preceding any solidification process. However, while there has been an extensive amount of theoretical and experimental work on solidification, the research on melting has attracted limited attention, mainly due to the fact that the microstructure of a material forms during solidification. Recently, however, melting has gained more interest, since in some technical applications, local remelting of partly solidified structures has been observed. Often, during a cooling process, a liquid of high-solute concentration or of higher temperature is transported by convection and brought into contact with a solid. This creates an out-of-equilibrium situation and can result in the remelting of the solid. Such remelting can occur in the mushy zone of a solidifying alloy, or during the joining of dissimilar metals and alloys. Local remelting has been identified as one of the main mechanisms for the fragmentation of dendrite arms[1] and for freckle formation in directionally solidified nickel-base superalloys.[2] It also plays an important role in the formation of inverse segregation (exudation) in continuous castings.[3] Understanding these phenomena requires a thorough understanding of remelting processes.

Some researchers have treated melting as the inverse process of solidification. Following the work on directional solidification and on accompanying phenomena such as constitutional undercooling or, in general, interface stability, theoretical studies on directional melting were carried out. These studies involved solving the diffusion equation in the solid instead of in the liquid.[4,5] The theoretical studies were accompanied by experiments in Sn-Sb[6] and in Sn-Bi[7] alloys.

Han and Hellawell[8] have qualitatively discussed the two ranges of melting-interface velocities that result from two different driving forces, *i.e.*, solute driven dissolution and thermally controlled remelting. For both types of driving forces, only a few theoretical and experimental studies have been carried out. Thermally controlled melting has been investigated by subjecting Sn-Bi particles[9] or Nb-Ti wires[10] to rapid heating. It appears that in these alloys a high level of superheating (or supersaturation) is achievable, while in pure materials, superheating is difficult to attain.[11] Some results are available for the isothermal melting of succino nitrile-water alloys.[12] The effects of convection and exothermic heat of mixing on the dissolution of ice in sulfuric acid and silicon in high-carbon steels have also been reported.[13] However, the present authors are not aware of any systematic study done on solute-driven melting.

An experimental method in which a pure solid and a highly alloyed liquid are brought into contact with well-defined initial conditions has been presented in an earlier work.[14] Melting starts with an interface that is far from equilibrium, and the interface position is tracked through a heat-balance calculation. The preliminary results indicate that even at low melting rates, local equilibrium is not necessarily achieved at the interface. In this study, the experimental setup presented in Reference 14 is used to systematically investigate the kinetics of solute-driven melting as a function both of supersaturation in the liquid and of temperature. Driving force and melting rate are correlated with empirical equations. The question of local equilibrium at the interface will be addressed in a separate article.[15]

## II. EXPERIMENTAL

In the remelting experiments, an Al-0.5 at. pct Fe alloy and Al-Mg alloys of various concentrations of Mg were

B. DUTTA, Research Associate, and M. RETTENMAYR, Senior Research Scientist, are with the Department of Materials Science, Technical University of Darmstadt, Petersenstrsse 23, Darmstadt 64287 Germany.

Manuscript submitted June 15, 1999.

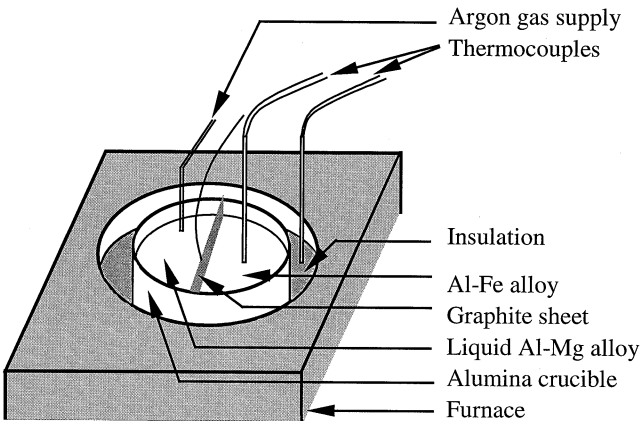


Fig. 1—Experimental setup.

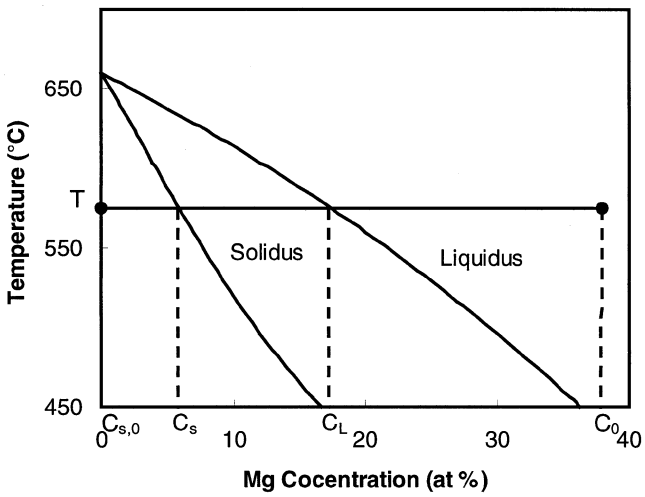


Fig. 2—Al-rich side of the Al-Mg phase diagram. Initial concentrations of the solid ($C_{0,S}$) and liquid ($C_0$) are marked on the figure along with the equilibrium solidus ($C_S$) and liquidus ($C_L$) compositions at an experimental temperature of $T$.

used as the solid and liquid materials, respectively. The reason for choosing an Al-Fe alloy for the melting component, instead of pure Al, is that, because the intermetallic compounds of Al and Fe precipitate between the dendrite arms, they provide a decoration of the microstructure that allows for the tracking of the interface positions at the end of the experiments. The extremely low solubility of Fe in solid Al is expected to have a negligible influence on the melting behavior of solid Al. Hence, the solid can be treated as pure Al. In addition, for the low Fe concentrations used in the present study, the liquidus and solidus isotherms in the ternary Al-Fe-Mg phase diagram are nearly parallel to each other and are perpendicular to the Mg concentration axis.[16] This implies that the liquidus temperatures of the Al-Mg system remain unaffected by the presence of small additions of Fe.

The rationale behind choosing Al-Mg alloys is that the density difference between Al and Mg is considerably smaller as compared to other well known Al alloys (such as Al-Zn, Al-Cu, *etc.*). For higher density differences, a high degree of segregation in the liquid is expected, leading to very different remelting velocities locally.[17]

Cylindrical samples of both alloys were cast in alumina crucibles. The mean sample diameter and height were both 55 mm. The samples were sectioned along their meridian planes and split into two equal halves. Subsequently, one-half of the Al-Fe alloy and one-half of the Al-Mg alloy were put together and placed in an alumina crucible. The two parts were separated by a graphite sheet 0.4 mm in thickness.

The crucible was placed inside a resistance-heating furnace and the gap between the crucible and the furnace inner wall was packed with ceramic fibers to minimize the heat flow across the perimeter of the sample. This ensured that the boundary conditions were as close to adiabatic as possible. Under these conditions, the consumption of latent heat during the melting process causes a temperature decrease in the sample. The large sample size ($\sim$ 130 $cm^3$) was chosen in order to obtain a signal of temperature stronger than the thermal noise (*i.e.*, the heat transfer through the insulation). A Ni/Ni-Cr thermocouple was inserted inside the Al-Fe sample, and a second thermocouple was placed at the inner wall of the furnace, for measuring the sample and furnace temperatures, respectively. The temperature-time data were recorded through a computer-interfaced data-acquisition system. The heat-transfer coefficient through the insulation was determined in each experiment during the heating of the sample. In one of the experiments, three thermocouples were placed at different depths inside the solid Al-Fe alloy to determine the temperature distribution along the vertical axis of the sample. In order to reduce the oxidation of the liquid Al-Mg alloy, Ar gas was purged through a ceramic tube on the top of the Al-Mg alloy sample. A schematic diagram of the experimental setup is shown in Figure 1.

The samples were heated to the required temperature $T$ (well above the liquidus temperature of the Al-Mg alloy, but below the melting point of the Al-Fe alloy) and allowed to stabilize for some time. The temperature and concentration chosen for a typical experiment are shown in Figure 2, to illustrate the experimental conditions. The experiment was initiated by the removal of the graphite sheet, thus generating an interface between the solid and liquid phases. After an initial incubation time, the solid started melting, with a consequent drop in temperature. The mean remelting rate was calculated from the temperature-time data. After some time (typically 100 to 300 seconds, depending on the experimental conditions), the furnace was opened and the solid was pulled out and quenched in water as quickly as possible.

The remelted surface of the quenched solid was photographed and the total area of remelting was measured using automatic image analysis (Quantimet software (LEICA, Imaging Systems Ltd., Cambridge, England)). Subsequently, the solid was sectioned vertically and the depth profile of the remelted surface was measured using a stereomicroscope. Three different sections were measured for each experiment and the average depth from these measurements was divided by the total time of remelting to obtain the average velocity of remelting for each experiment. From here on in this article, this velocity is referred to as the geometric velocity. Sections of the quenched samples were polished and their microstructures were studied using an optical microscope.

**Table I. Values of Specific Heat and Heat of Fusion Used for Calculating the Interface Velocity during Remelting**

| Specific Heat ($J/m^3/K$) | | | | | Heat of Fusion of Solid Al ($J/m^3$) |
|---|---|---|---|---|---|
| Al Solid | Al Liquid | Mg Solid | Mg Liquid | $Al_2O_3$ Crucible | |
| $3.06 \times 10^6$ | $2.58 \times 10^6$ | $2.23 \times 10^6$ | $1.88 \times 10^6$ | $3.71 \times 10^6$ | $9.5 \times 10^8$ |

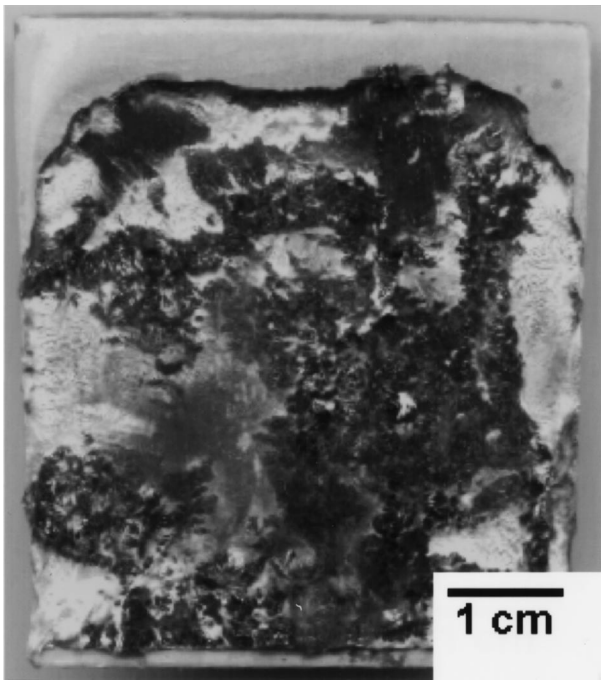


Fig. 3—Front view of the remelted sample.

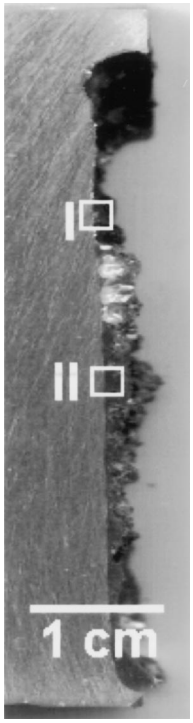


Fig. 4—Side view of a vertical section of the sample showing the profile of the melted region.

## III. CALCULATING THE INTERFACE VELOCITY DURING REMELTING

The interface velocity during remelting is calculated from the temperature-time data using a simple heat balance, given as

$$v_i = \frac{c_p V_t}{\Delta H A}\left[\frac{(T_f - T_s)_{r,i}}{(T_f - T_s)_h}\left(\frac{\Delta T}{\Delta t}\right)_h - \left(\frac{\Delta T}{\Delta t}\right)_r\right] \qquad [1]$$

where $v_i$ is the remelting velocity at the $i$th time interval; $c_p$ and $V_t$ are the specific heat and total volume of the sample, respectively; $A$ is the area of remelting; $\Delta H$ is the heat of fusion of the solid; $T_f$ and $T_s$ represent the furnace and sample temperature, respectively; and the subscripts $h$ and $r$ indicate the temperatures during heating and remelting, respectively. Thus, $(\Delta T/\Delta t)_h$ and $(\Delta T/\Delta t)_r$ represent the heating and cooling rate of the sample. The details of this derivation can be found elsewhere.[14] The values of the specific heats of the liquid and the solid and of the heat of fusion of the solid used in the calculation are given in Table I.

## IV. RESULTS

In Figure 3, a typical picture of the surface of a remelted sample is shown. The area of remelting ($A$ in Eq. [1]) is measured from similar photographs for each experiment. The black patches in the picture are the parts of the oxide skin on the top of the liquid Al-Mg alloy that may have gotten stuck on the sample during its removal from the furnace. In addition to this, there is a layer of liquid adherent to the remelted surface of the solid, which is shown in more detail in the quenched microstructures (Figures 5(a) and (b)). Figure 4 shows the side view of a vertical section from a solid sample. The profile of the remelted region can be clearly seen here. From the figure, it is evident that the depth of remelting gradually increases from the bottom of the sample toward the top; this issue will be discussed later in this article. It can be noted that the geometric velocity is an average of the remelting depth from the bottom to the top, divided by the total duration of remelting. The microstructures at two locations of the sample (I and II in Figure 4) are shown in Figures 5(a) and (b). The $FeAl_3$ particles decorating the interdendritic regions of the solid mark the boundary between the pre-existing solid and quenched liquid. The adhesive layer of the quenched liquid is found to have different thicknesses at different places, *e.g.*, a thicker layer in Figure 5(a) as compared to that in Figure 5(b). Thus, the presence of $FeAl_3$ particles facilitates a precise

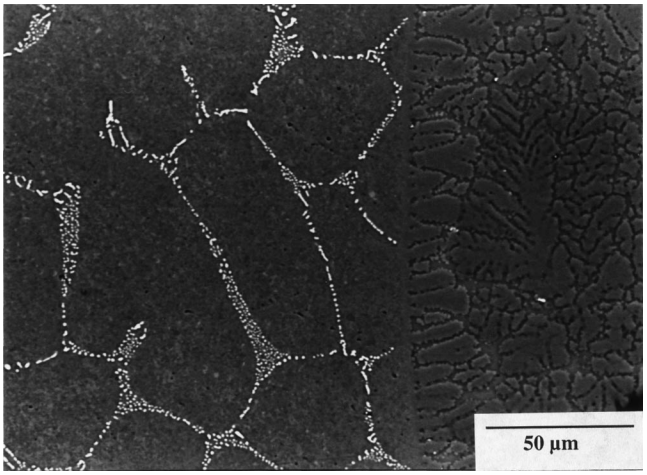


(*a*)

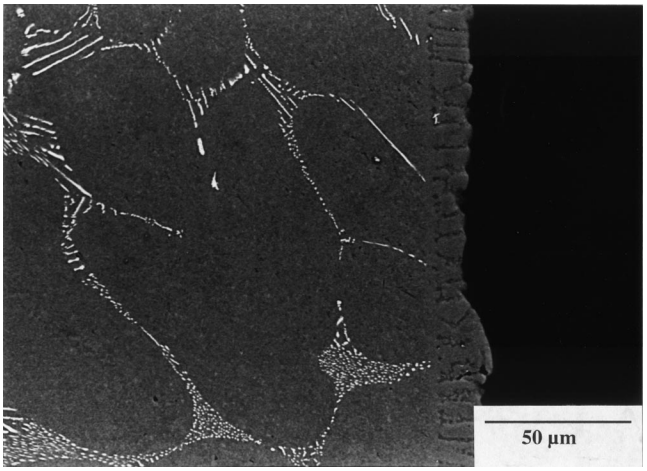


(*b*)

Fig. 5—(*a*) and (*b*) Micrographs of the interface from regions I and II, respectively, of the sample shown in Fig. 4. Presence of interdendritic $FeAl_3$ particles in the solid mark the exact location of the solid/liquid interface. A thick adhesive layer of the quenched liquid is shown in (a), while a thin adhesive layer on the solid is shown in (b).

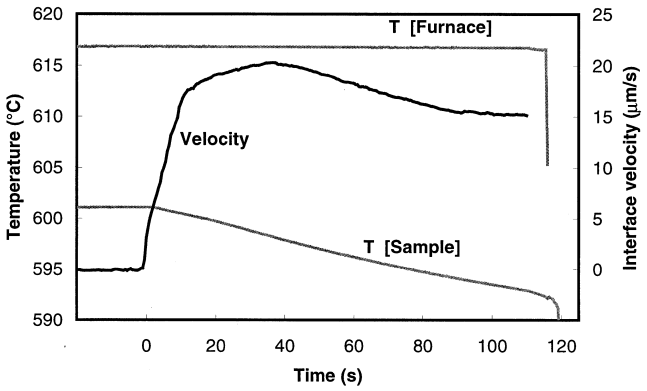


Fig. 6—Variation of sample and furnace temperature with time during remelting. Corresponding interface velocity as calculated from the heat balance equations is also plotted.

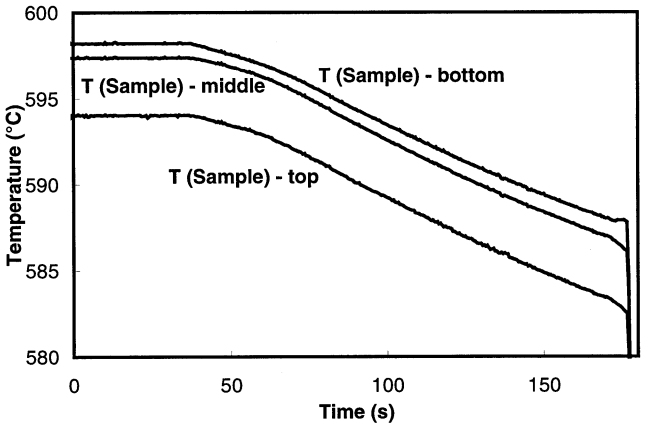


Fig. 7—Variation of temperature at different depths in the sample.

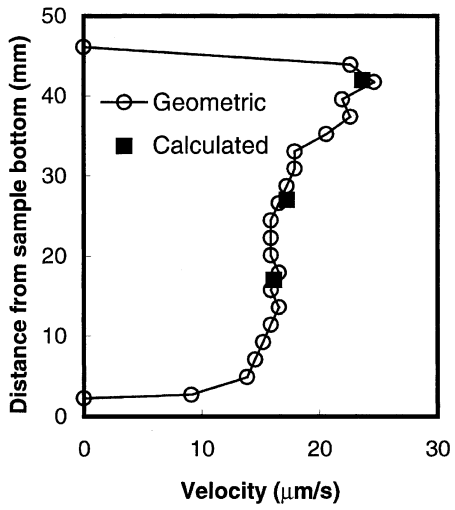


Fig. 8—Variation of remelting velocity across the height of the sample. A picture of a vertical section showing the profile of the remelted surface is also shown (average $T$ = 597 °C, $C_0$ = 32 at. pct).

determination of the position of the interface after quenching and enables an accurate measurement of the geometric velocity.

In Figure 6, the variation in the sample and furnace temperatures during remelting is shown as a function of time. The decrease of the sample temperature is a result of remelting, as mentioned earlier. It should be noted that the furnace temperature remains almost constant during the entire experiment, indicating the attainment of a very stable condition for the furnace. The velocity of the remelting interface, calculated using the heat balance (Eq. [1]), is also shown in this plot. After a short incubation period, the remelting begins and the velocity steeply increases to a maximum. Further continuation of the experiment leads to a gradual decrease in the remelting velocity until the end of the experiment.

Due to the Ar gas stream, there is a slight temperature gradient from the bottom to the top in the sample, as indicated by the measured temperatures at three different locations, particularly at the bottom, the middle, and the top part of the solid sample (Figure 7). The interface velocities corresponding to these three regions have been calculated from the time-temperature data. The results are shown in Figure 8. The geometric velocity, as measured from the depth profile

**Table II. Initial Temperature ($T$), Initial Composition ($C_0$), Temperature Drop ($\Delta T$), Time Duration ($\Delta t$), Geometric Velocity ($v_{geo}$), and Calculated Velocity ($v_c$)**

| Sample | $C_0$ (at. Pct) | $T$ (°C) | $\Delta T$ (K) | $\Delta t$ (s) | $v_{geo}$ ($\mu$m/s) | $v_c$ ($\mu$m/s) |
|---|---|---|---|---|---|---|
| 1 | 30.1 | 555.9 | 3.2 | 251 | 3.4 | 3.8 |
| 2 | 20.7 | 573.0 | 1.9 | 382 | 2.3 | 1.9 |
| 3 | 25.1 | 576.9 | 1.6 | 87 | 8.6 | 8.6 |
| 4 | 21.2 | 587.9 | 1.4 | 206 | 6.9 | 7.8 |
| 5 | 32.2 | 596.8 | 10.3 | 136 | 17.3 | 17.6 |
| 6 | 22.4 | 597.3 | 1.7 | 68 | 12.1 | 10.4 |
| 7 | 22.4 | 599.5 | 1.2 | 80 | 10.0 | 11.5 |
| 8 | 16.8 | 600.4 | 2.8 | 243 | 4.2 | 4.4 |
| 9 | 30.1 | 601.1 | 8.1 | 111 | 16.6 | 16.9 |
| 10 | 36.1 | 603.4 | 8.6 | 99 | 20.7 | 21.6 |
| 11 | 20.5 | 604.9 | 4.5 | 237 | 10.6 | 11.8 |
| 12 | 20.4 | 609.8 | 9.4 | 405 | 16.2 | 14.6 |
| 13 | 20.5 | 610.1 | 6.7 | 119 | 13.8 | 15.1 |
| 14 | 16.8 | 626.4 | 3.4 | 223 | 20.1 | 21.0 |

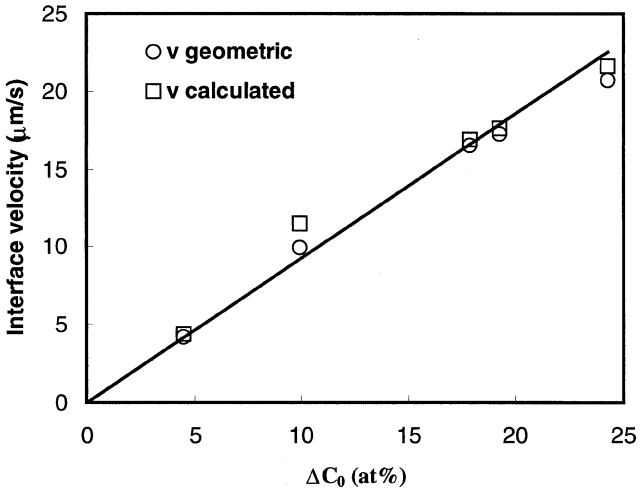


Fig. 9—Variation of remelting velocity as a function of liquid supersaturation ($\Delta C_0$) at a constant temperature ($T \approx 600$ °C).

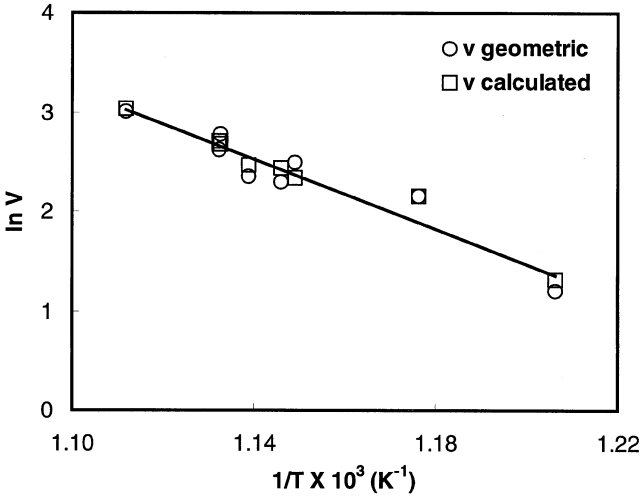


Fig. 10—Variation of remelting velocity ($\mu$m/s) as a function of inverse of temperature at a constant liquid supersaturation ($\Delta C_0 \approx 10$ at. pct).

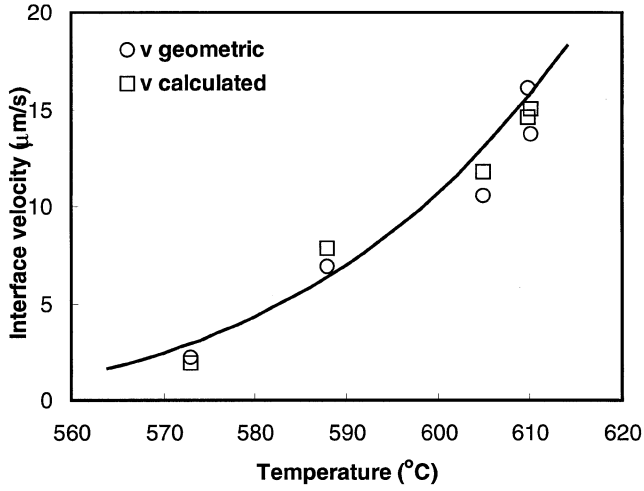


Fig. 11—Variation of remelting velocity as a function of temperature at a constant initial liquid composition ($C_0 \approx 21$ at. pct).

of the corresponding sample, is also shown in this figure. Clearly, the remelting velocity is lowest at the bottom and highest at the top. In addition, the calculated velocities are found to be in excellent agreement with the measured velocities.

In Table II, the experimental conditions used in the present study are listed together with the resultant velocity values. It should be noted that, unlike in the previous case (Figure 8), the velocities tabulated here represent the mean velocity for the entire sample and not for any particular location. In general, the agreement between the calculated velocity and the geometric velocity, directly measured from the sample, is found to be excellent in almost all of the experiments. However, at lower interface velocities, the relative difference between the two interface velocities is found to be larger than that at higher interface velocities.

At a constant temperature of $T \approx 600$ °C, the remelting velocity varies as a function of the liquid supersaturation ($\Delta C_0 = C_0 - C_L$), as shown in Figure 9. Both the calculated velocity $v_c$ and the geometric velocity $v_{geo}$ are shown. It is found that the remelting velocity increases linearly with increasing liquid supersaturation. A mathematical fit yields the following relation between the interface velocity and liquid supersaturation:

$$v = 0.929\ \Delta C_0 \qquad [2]$$

The correlation coefficient is, $\gamma^2 \approx 0.96$.

At a constant supersaturation ($\Delta C_0 \approx 10$ at. pct), *i.e.*, a constant driving force, the melting process is controlled by the kinetic, which, in turn, is a function of temperature. Figure 10 is an Arrhenius-type plot, showing the variation of the remelting velocity as a function of the inverse of temperature ($1/T$) at a constant liquid supersaturation. The velocity increases exponentially with increasing temperature. An exponential fit to the experimental data yields the following relation between the interface velocity $v$ (in $\mu$m/s) and temperature $T$ (in K):

$$v = 3.2 \times 10^9 \exp\left(-\frac{17{,}000}{T}\right) \qquad [3]$$

The correlation coefficient is, $\gamma^2 \approx 0.98$ for this fit.

Figure 11 is a plot of interface velocity as a function of

temperature, at a constant initial liquid composition $C_0$. Thus, an increase in temperature indicates an associated increase in liquid supersaturation. The results reveal an increase of the remelting velocity with an increase in temperature.

## V. DISCUSSION

The experimental setup used in this work provides an excellent tool for studying remelting. The initial and boundary conditions are well defined, and the results are consistent. Setting the boundary conditions to adiabatic allows for the determination of the time-dependent remelting velocity ($v_c$). The average $v_c$ is verified by the $v_{geo}$, determined from the volume loss of the sample. Overall, the agreement between the two velocities $v_c$ and $v_{\text{geo}}$ is very good. Their relative difference is larger at lower interface velocities, a fact that can easily be attributed to a possible measurement error when the remelting depth is small. Nevertheless, the results indicate that the present technique is a potential method for tracing the interface velocity, and they also confirm the reliability of the heat-balance calculations.

The variation of the interface velocity with time, as shown in Figure 6, depicts the entire process of remelting. The small incubation time that occurs before the actual process of remelting can be attributed to the time taken for the dissolution of the oxide layer that forms on the surface of the solid during heating. It is reasonable to assume that the remelting begins locally at a small area, and this area then spreads until it covers the entire contact surface of the samples. During this period, the interface velocity increases and reaches the maximum when a complete contact between the solid and liquid is established. From this point onward, the interface velocity continuously decreases with time. The concentration gradient in the liquid at the interface provides a solute flux toward the solid that maintains the driving force for remelting. In the course of the experiment, the liquid concentration at the interface decreases and tends toward the equilibrium liquid concentration (or concentration values that are even lower, in the case of the loss of equilibrium[15]). This leads to a decrease in the concentration gradients, which, in turn, slows down the remelting velocity.

The temperature gradient in the sample is not significant, either locally or globally, for the measured remelting velocities. According to the temperature measurements, there is a temperature decrease from the bottom to the top of the sample (Figure 7). This could result in a corresponding decrease of the interface velocity from the bottom toward the top of the sample. However, the results of the velocity variation across the sample length clearly reveal an opposite trend in the sample, *i.e.*, the velocity increases from the bottom toward the top of the sample (Figure 8). This is attributed to the gravity-induced segregation of Mg toward the top of the liquid. The thermosolutal convection in the melt, due to the density difference between Mg and Al, can lead to concentration differences of as much as 7.5 at. pct from the bottom to the top (*e.g.*, $c = 13$ at. pct at the bottom and 20.5 at. pct at the top), as a numerical investigation reveals.[15,18] The segregation of Mg, in turn, changes the supersaturation locally; hence, the driving force is maximum at the top and gradually decreases toward the bottom. The resulting effect is clearly manifested by the variation in the remelting velocity across the height of the sample. Thus, the change of supersaturation due to segregation is the dominant factor for the observed interface-velocity profile.

Because the liquid supersaturation is the driving force for the melting, it is not surprising that an increase in the solute content in the liquid accelerates the remelting rate. A linear relationship between the initial supersaturation and the interface velocity was observed and analyzed earlier in the case of solid-state transformations (precipitate growth) with an incoherent planar interface.[19] As expected, the interface velocity is found to increase with the temperature at a constant driving force (liquid supersaturation). The reasons for the acceleration are twofold. First, a higher temperature implies a higher diffusion coefficient, and thus aids a faster mass transport in both the solid and the liquid. Second, a higher temperature decreases the viscosity (increases the fluidity) of the liquid, facilitating mass transport in the liquid by convection.

Thermosolutal convection is expected to be a prominent mechanism controlling the remelting rate in this type of experiment. The temperature gradient in the solid (and hence in the liquid) induces thermal convection in the liquid that could only be suppressed with sample sizes on the order of a few millimeters.[20] In the experiments presented here, a much larger sample size (sample radius $\sim$27 mm, sample height $\sim$55 mm) was chosen in order to get a temperature signal stronger than the thermal noise entering the sample from the furnace. Additionally, solutal convection is a consequence of the density difference of the alloy components (refer also to the numerical calculations in References 15 and 18). Mg, as the lighter element, tends to segregate toward the top of the sample. It is well known that both the increase of diffusivity and the decrease of viscosity are exponential functions of temperature. Therefore, the velocity was fitted with an Arrhenius type of relationship, yielding an acceptable correlation. The liquid diffusion coefficient of Mg in Al is given as[21]

$$D_\ell = 9.9 \cdot 10^{-5} \exp\left[-\frac{8610}{T}\right] \qquad [4]$$

The normalized activation energy for solute diffusion is only about half of the corresponding value in Eq. [3]. Thus, the dependence of the remelting rate cannot be attributed to solute diffusion as the governing mechanism and indicates that the convection plays a predominant role in mass transport.

As shown in Figure 10, the interface velocity increases exponentially with increasing temperature for constant supersaturation. This can be written as

$$v = K_0 \exp\left(-\frac{Q}{T}\right) \qquad [5]$$

where $K_0$ is a pre-exponential factor and $Q$ is an activation energy for mass transport. Comparing Eqs. [3] and [5] yields the values of $K_0$ and $Q$ as $3.2 \times 10^9$ and 17,000, respectively, for these experiments. The interface kinetics during the continuous growth of a rough interface can be expressed as a product of a factor involving the thermodynamic driving force and a kinetic prefactor representing interface mobility.[22] Incorporating the effect of liquid supersaturation, *i.e.*, the thermodynamic driving force (as obtained from Eq. [2]) in Eq. [5] leads to

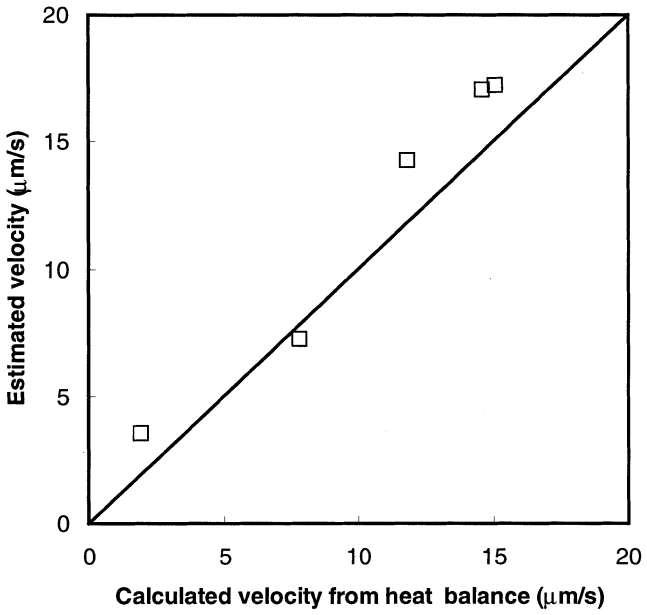


Fig. 12—A comparison of the interface velocities predicted by Eq. 9 and those calculated from the heat balance equation.

$$v = K_C \Delta C_0 \, K_K \exp\left(-\frac{Q}{T}\right) \qquad [6]$$

where $K_C$ is a constant correlating the chemical driving force (arising due to $\Delta C_0$) with the interface velocity, and $K_K$ is a kinetic constant ($K_K = K_0/K_C \Delta C_0$).

Inserting the values of $K_0$ ($=3.2 \times 10^9$), $K_C$ ($=0.929$ from Eq. [2]), and $\Delta C_0$ ($=10$) yields the value of $K_K$ as $3.446 \times 10^8$ in this study. The first two terms in Eq. [6] represent the effect of supersaturation (the thermodynamic driving force), and the last two terms represent the effect of temperature (the kinetic factor) on the interface velocity.

Now, consider the effect of temperature on the interface velocity at a constant initial liquid composition, as shown in Figure 11. This represents a typical case where both the thermodynamic driving force and the temperature are variables that have a combined effect on interface velocity. Substituting $\Delta C_0$ in Eq. [6] by $\Delta T_0/m_L$ leads to

$$v = K_C \frac{\Delta T_0}{m_L} K_K \exp\left(-\frac{Q}{T}\right) \qquad [7]$$

where $\Delta T_0$ is the difference in the liquidus temperature corresponding to the $\Delta C_0$ difference in the liquid composition and $m_L$ is the slope of the liquidus in the Al-Mg phase diagram. The variable $\Delta T_0$ is given as $(T - T_L)$, where $T_L$ is the equilibrium liquidus temperature. For a constant initial liquid composition $C_0$, $T_L$ can be replaced by $(T_M - m_L C_0)$, where $T_M$ is the melting temperature of pure Al. Rewriting Eq. [7] yields

$$v = \frac{K_C \, K_K}{m_L} \{T - (T_M - m_L C_0)\} \exp\left(-\frac{Q}{T}\right) \qquad [8]$$

Inserting the values of $K_C$ (0.929), $K_K$ ($3.446 \times 10^8$), $m_L$ (5.766 *K*/at. pct), $T_M$ (933 K), and $Q$ (17,000 J/mol) gives the variation of the interface velocity as a function of temperature at a constant initial liquid composition as

$$v = 5.552 \times 10^7 \{T - (933 - 5.766 \, C_0)\} \exp\left(-\frac{17{,}000}{T}\right) \qquad [9]$$

Figure 12 is a comparison of the interface velocities predicted by Eq. [9] and those calculated using the heat-balance formulation (Eq. [1]) for the case of constant liquid composition (*i.e.*, $C_0 = 21$ at. pct). The results show a reasonably good agreement between the values predicted by Eq. [9] and those calculated from the heat balance. This clearly indicates that the empirical relations described earlier are able to estimate the effects of the liquid supersaturation and temperature on the interface velocity in the range of compositions and temperatures studied here.

## VI. CONCLUSIONS

A systematic study has been carried out to investigate the kinetics of remelting (*i.e.*, the velocity of a remelting interface) as a function of temperature and supersaturation. The interface velocities during remelting have been determined by a heat balance via the temperature decrease, and geometrically via the volume loss. The agreement between these two velocities is found to be excellent. The following conclusions are drawn

1. At a constant temperature, the remelting velocity is a linear function of liquid supersaturation.
2. At a constant liquid supersaturation, the interface velocity increases exponentially with increasing temperature.
3. A constant initial concentration leads to a faster increase in the interface velocity with increasing temperature, as the effects of driving force and kinetics are combined.
4. In the present experiments, the driving force for remelting, the local supersaturation, is mainly set by thermosolutal convection.
5. A set of empirical relations has been developed to account for the effects of liquid supersaturation and temperature on the interface velocity. A combined analysis of these two effects yields a relation for the interface velocity as a function of temperature that reproduces the experimental observations satisfactorily.

The results of the present investigation are expected to aid the development of a consistent thermodynamic and kinetic model for describing remelting phenomena.

## ACKNOWLEDGMENTS

This work is part of the project "Modelling of Processes in Materials Production" in COST 512 "Modelling in Materials Science and Processing." Sponsorship by the German Ministry of Research under Project No. 03K 8003 is gratefully acknowledged. The authors are thankful to Professor H.E. Exner, Technical University of Darmstadt, for helpful discussions.

## REFERENCES

1. A. Hellawell, S. Liu, and S.Z. Lu: *J. Met.*, 1997, vol. 49, pp. 18-20.
2. M.C. Schneider, J.P. Gu, C. Beckermann, W.J. Boettinger, and U.R. Kattner: *Metall. Mater. Trans. A*, 1997, vol. 28A, pp. 1517-31.

3. E.E. Emley: *Int. Metall. Rev.*, 1976, vol. 21, pp. 75-115.
4. D.P. Woodruff: *Phil. Mag.*, 1968, vol. 17, pp. 283-94.
5. J.D. Verhoeven and K.A. Heimes: *J. Cryst. Growth*, 1971, vol. 10, pp. 179-84.
6. J.D. Verhoeven and E.D. Gibson: *J. Cryst. Growth*, 1971, vol. 11, pp. 29-38.
7. J.D. Verhoeven and E.D. Gibson: *J. Cryst. Growth*, 1971, vol. 11, pp. 39-49.
8. Q. Han and A. Hellawell: *Metall. Mater. Trans. B*, 1997, vol. 28B, pp. 169-73.
9. W.P. Allen, H.J. Fecht, and J.H. Perepezko: *Scripta Metall.*, 1989, vol. 23, pp. 643-48.
10. D. Basak, W.J. Boettinger, D. Josell, S.R. Coriell, J.L. McClure, S. Krishnan, and A. Cezairliyan: *Acta Mater.*, 1999, vol. 47, pp. 3147-58.
11. J. Daeges, H. Gleiter, and J.H. Perepezko: *Phys. Lett.*, 1986, vol. A119, pp. 79-82.
12. X. Wan, Q. Han, and J.D. Hunt: *Metall. Mater. Trans. A*, 1998, vol. 29A, pp. 751-55.
13. H. Hu and S.A. Argyropoulos: *Metall. Mater. Trans. B*, 1997, vol. 28B, pp. 135-48.
14. M. Rettenmayr, O. Warkentin, and H.E. Exner: *Z. Metallkd.*, 1997, vol. 88, pp. 617-19.
15. M. Rettenmayr, O. Warkentin, M. Rappaz, and H.E. Exner: unpublished research.
16. G. Petzow: in *Ternary Alloys: A Comprehensive Compendium of Evaluated Constitutional Data and Phase Diagrams*, G. Petzow and G. Effenberg, eds., VCH, Weinheim, 1992, vol. 5, pp. 244-45.
17. D.J. Hebditch and J.D. Hunt: *Metall. Trans.*, 1974, vol. 5A, pp. 1557-64.
18. M. Retternmayr, O. Warkentin and M. Rappaz: in *Solidification and Gravity 2000*, A. Roósz, M. Rettenmayr, and D. Watring, eds., Materials Science Forum, Trans Tech Publications, Uetikon, Switzerland, 2000, vols. 329–330, pp. 339-44.
19. D.A. Porter and K.E. Easterling: *Phase Transformations in Metals and Alloys*, VanNostrand Reinhold Int., London, 1981.
20. G.S. Cole: *Solidification*, ASM Seminar Series, ASM, Metals Park, OH, 1971, p. 201.
21. K. Kovakova and M. Sipocz: in *DIMETA 2, Proc. Int. Conf. on Diffusion in Metals and Alloys*, F.J. Kedves and D.L. Beke, eds., Trans Tech Publications, Aedermannsdorf, Switzerland, 1982, p. 533.
22. H. Biloni and W.J. Boettinger: in *Physical Metallurgy*, 4th ed., R.W. Cahn and Peter Haasen, eds., North-Holland, Amsterdam, 1996, vol. 1, p. 704.